Supplementary Information (SI) for Journal of Materials Chemistry A.
This journal is © The Royal Society of Chemistry 2025

Optimization of $CoFe_2O_4$ electronic structure by reticulate expanded graphite to accelerate non-radical activation of peroxymonosulfate for efficient antibiotic degradation in wastewater

Qi Zhao [a], Weiguang Li [a,b,*], Shangfeng Jiang [a], Jingyi Zhang [a], Longyi Lv [c]
Caihua Bai [a], Xuhui Wang [a,*]

[a] School of Environment, Harbin Institute of Technology, Harbin 150090, China
[b] State Key Laboratory of Urban Water Resource and Environment, Harbin Institute of Technology, Harbin 150090, China
[c] Tianjin Key Laboratory of Clean Energy and Pollution Control, School of Energy and Environmental Engineering, Hebei University of Technology, Tianjin 300401, China

[*]Corresponding authors:
Weiguang Li
State Key Laboratory of Urban Water Resource and Environment, School of Environment, Harbin Institute of Technology, 73 Huanghe Road, Harbin, Heilongjiang 150090, China (E-mail: hit_lwg@126.com).
Xuhui Wang
School of Environment, Harbin Institute of Technology, 73 Huanghe Road, Harbin, Heilongjiang 150090, China (E-mail: xuhuilcg@126.com).

Captions

Text S1. Details of agents.

Text S2. Theoretical calculation methods.

Text S3. Effects of used $CoFe_2O_4$-EG after thermal activation regeneration

Text S4. TC degradation pathway.

Fig. S1. Effects of $CoFe_2O_4$-EG after thermal activation regeneration.

Fig. S2. Oxidative degradation pathways of TC

Fig. S3. MS/MS spectra of products detected by UHPLC-QTOF/MS.

Table.S1 Possible TC degradation intermediates in the $CoFe_2O_4$/EG/PMS system

Text S1. Details of agents.

Expandable graphite was obtained from Nanjing Grefa Carbon Materials Co., Ltd. 5,5-dimethyl-1-pyrroline-N-oxide (DMPO, AR), 2,2,6,6-Tetramethyl-4-piperidone (TEMP, AR), and sodium bicarbonate ($NaHCO_3$, AR) were purchased from Aladdin Chemical Reagent Co., Ltd. Peroxymonosulfate ($KHSO_5$, PMS, AR), methanol (MeOH, AR), ethanol (EtOH), phenol (PhOH, AR), and tetracycline (TC, AR) were obtained from Shanghai Macklin Biochemical Technology Co., Ltd. (Shanghai, China). Ferric nitrate hexahydrate ($Fe(NO_3)\cdot 9H_2O$, AR), cobaltous nitrate hexahydrate ($Co(NO_3)_2\cdot 6H_2O$), sodium chloride (NaCl, AR), potassium chloride (KCl, AR), dibasic sodium phosphate (Na_2HPO_4, AR), sodium Bicarbonate ($NaHCO_3$, AR), and sodium thiosulfate ($Na_2S_2O_3$, AR) were purchased from Tianjin Kermel Chemical Reagent Co., Ltd.

Text S2. Theoretical calculation methods.

Density function theory calculations were conducted by Vienna ab initio simulation package (VASP). The core electrons were described by the projector-augmented plane wave (PAW) [1, 2]. The Perdew-Burke-Ernzerhof (PBE) was adopted as functional with the exchange-correlation term of generalized gradient approximation (GGA) [3]. In addition, the Bader charge was calculated through the algorithm BADER CHARGE ANALYSIS [4].

An adsorption model consisted of a slab model ($CoFe_2O_4$, $CoFe_2O_4$-EG) and a molecular model of HSO_5^- covered on the slab. Two electrons were localized around atomic group $SO_5^{\bullet -}$ to form HSO_5^- by adding two hydrogen atoms as counter ions. The cutoff energy for the plane wave basis was set at 450 eV with a 2 × 2 × 1 k-point grid for Brillouin zone sampling. A 30 Å vacuum layer was established to prevent interlayer interactions. The long-range van der Walls interactions were corrected by the DFT-D3 method [5].

The adsorption energy (E_{ads}) of adsorbate on the catalyst was calculated based on Equation 1 [6].

$$E_{ads} = E_{catalyst+adsorbate} - E_{catalyst} - E_{adsorbate} \quad (3)$$

where E_{ads} refers to the adsorption energy, eV; $E_{catalyst+adsorbate}$ is the total energy of catalyst slab and adsorbate, eV; $E_{catalyst}$ means the energy of the catalyst slab, eV; and $E_{adsorbate}$ is the energy of adsorbate, eV.

Pseudo-first-order kinetic (Equation 2) was applied to fit the oxidation processes of TC (data for 0-60 min) and calculate the corresponding degradation rate constants (k) [7].

$$ln\frac{C_t}{C_0} = -kt \quad (4)$$

where C_0 means the concentration of TC at the start of oxidation, mg/L; C_t means the concentration of TC at a point of oxidation, mg/L; t refers to the oxidation time ($0 \leq t \leq 60$), min.

Text S3. Effects of used $CoFe_2O_4$-EG after thermal activation regeneration

The used catalyst was regenerated through thermal activation at 300°C and compared with a standalone PMS system under identical conditions. Experimental results revealed that this method restored catalytic efficiency to over 70% of its initial level (Fig. S1), highlighting its remarkable reusability and practical applicability.

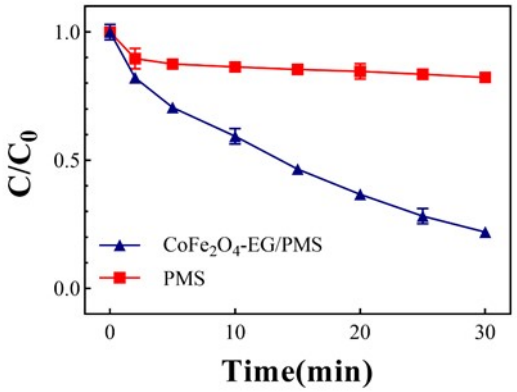

Fig. S1. Effects of used $CoFe_2O_4$-EG after thermal activation regeneration.

Text S4. TC degradation pathway.

To further investigate the reaction mechanism of TC, the intermediates were analyzed using UHPLC-QTOF/MS, and possible molecular structures were shown in Fig. 12. In the $CoFe_2O_4$-EG/PMS system, eleven major intermediates were detected with mass peaks at 460 (P1), 477 (P2), 379 (P3), 427 (P4), 371 (P5), 320 (P6), 302 (P7), 219 (P8), 279 (P9), 228 (P10), and 150 (P11). Based on the intermediates from the degradation of TC, a degradation pathway for TC was proposed. TC molecules were attacked by $SO_4^{\bullet-}$, $HO^{\bullet}$, and $^1O_2$, leading to the formation of low-molecular-weight products. TC under ultimate oxidation conditions, TC molecules might be oxidized and decomposed into two intermediate products, P1 and P2. During the reaction, TC molecules lose hydroxyl (-OH) groups, forming a new intermediate product P4. Simultaneously, P4 is converted to P3 by introducing an amino ($-NH_2$) group. P4 molecules were further oxidized to form P5. P4 and P5 molecules underwent ring-opening reactions to generate new intermediate products, P6 and P7. P7 underwent catalytic oxidation to form smaller molecules P8, P9, P10, and P11. Some intermediates were ultimately mineralized to CO_2 and H_2O.

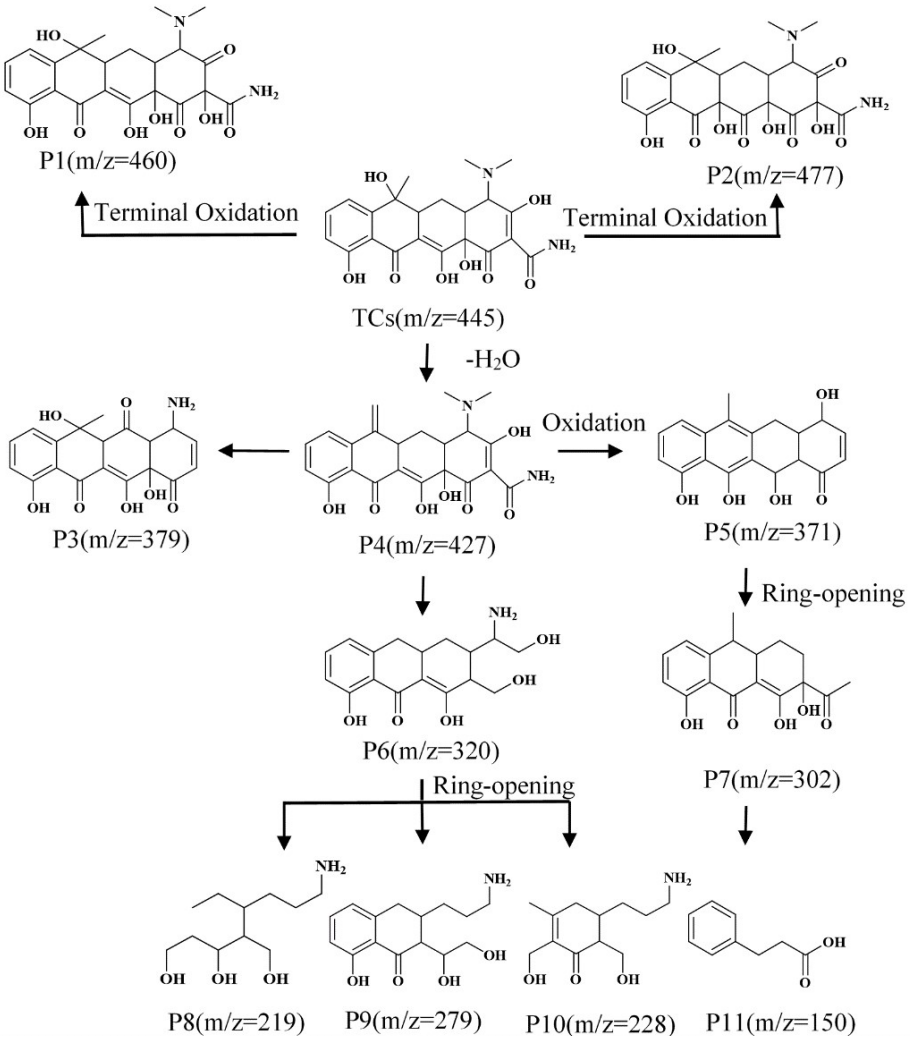

Fig.S2. Oxidative degradation pathways of TC

The chemical properties and secondary mass spectra of 11 intermediates are listed in Table S1.

Table S1. Possible TC degradation intermediates in the $CoFe_2O_4$-EG/PMS system.

Compound	Molecular formula	m/z (Molecular weight)	Molecular structure
P1	$C_{22}H_{24}N_2O_9$	460.44	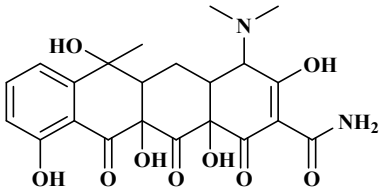
P2	$C_{22}H_{24}N_2O_{10}$	476.44	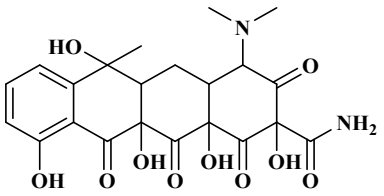
P3	$C_{19}H_{17}NO_7$	371.35	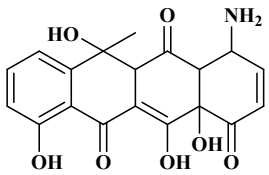
P4	$C_{15}H_{21}NO_4$	279.34	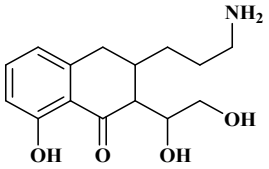
P5	$C_{19}H_{18}O_5$	326.35	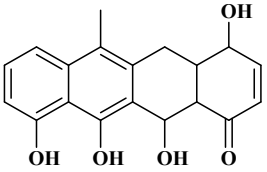
P6	$C_{17}H_{21}NO_5$	319.36	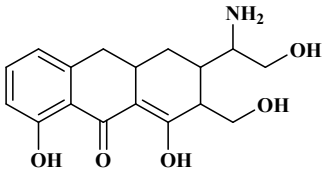

P7	$C_{17}H_{18}O_5$	302.33	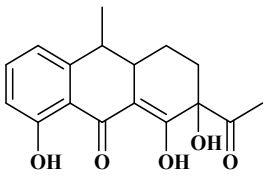
P8	$C_{11}H_{25}NO_3$	219.33	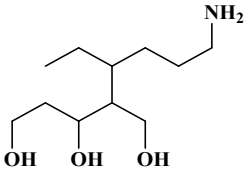
P9	$C_{15}H_{21}NO_4$	279.34	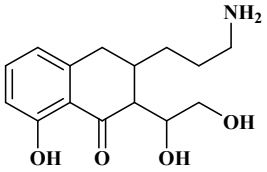
P10	$C_{12}H_{21}NO_3$	227.30	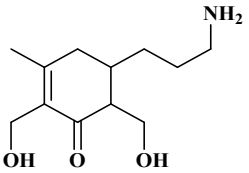
P11	$C_9H_{10}O_2$	150.18	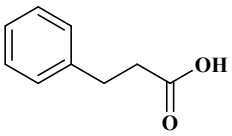

a

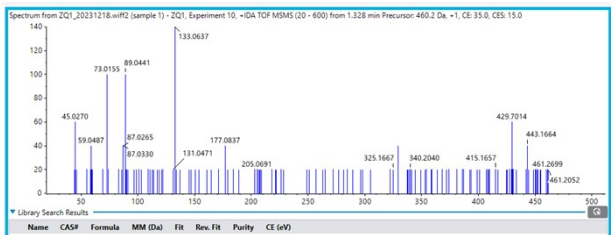

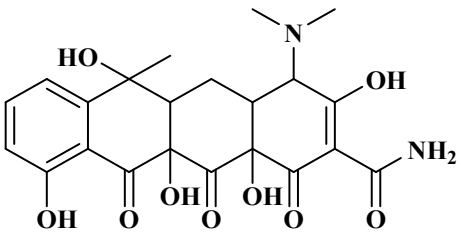

P1

b

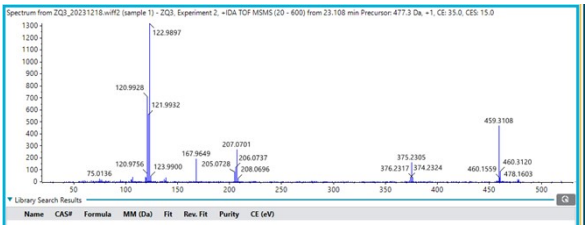

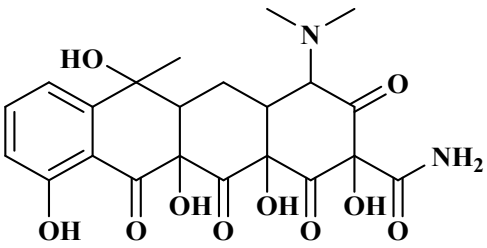

P2

c

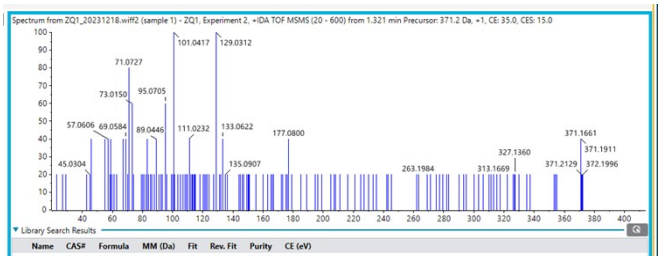

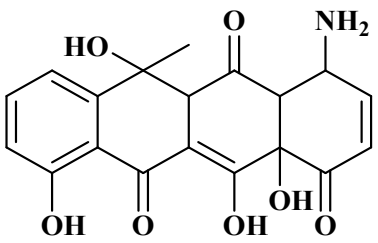

P3

d

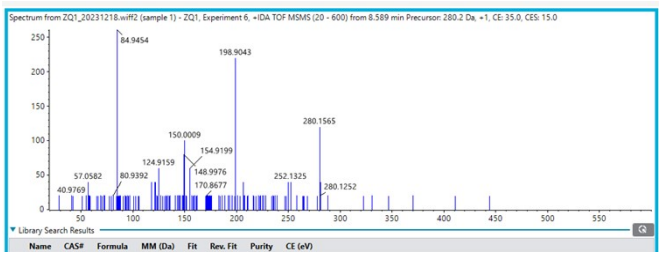

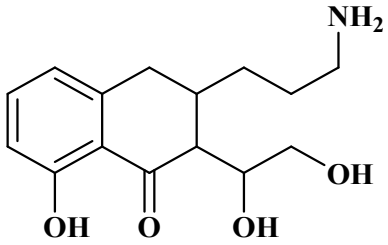

P4

e

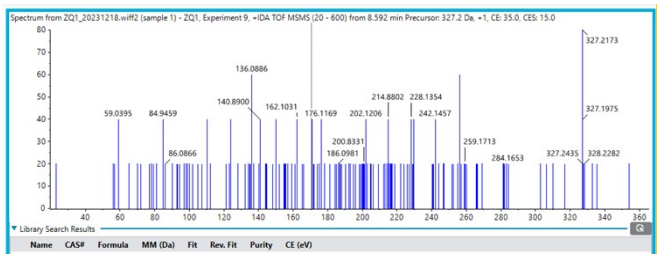

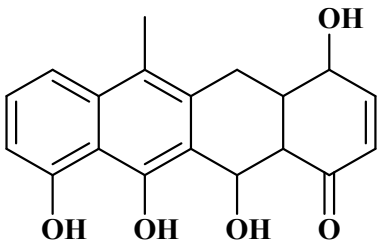

P5

f

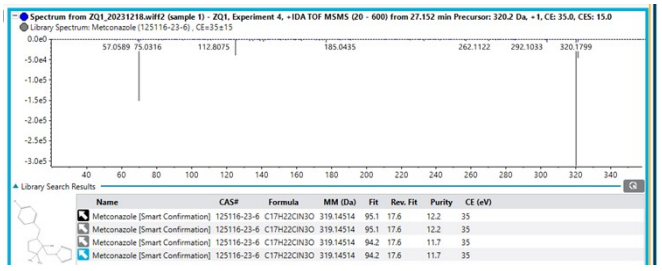

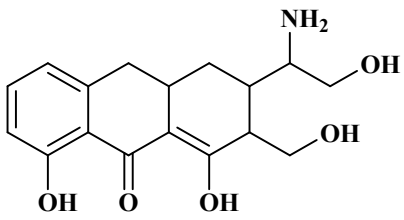

P6

g

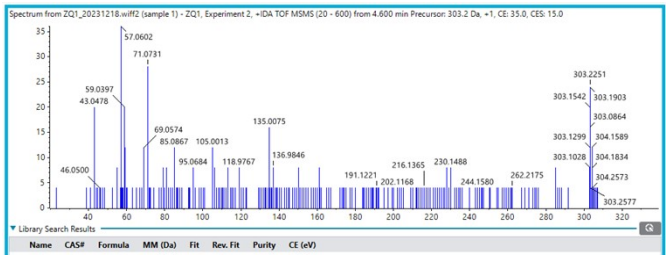

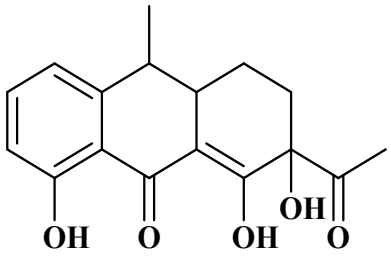

P7

h

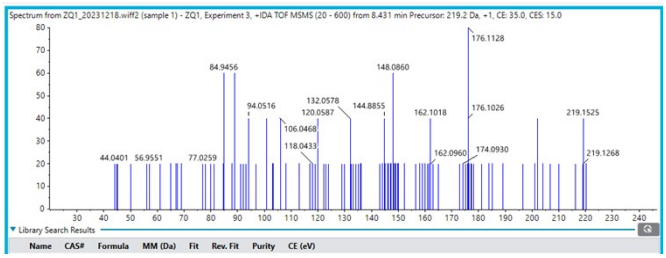

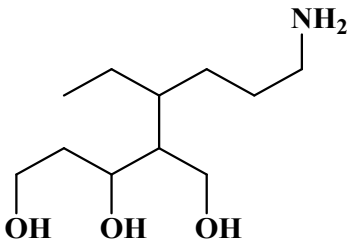

P8

i

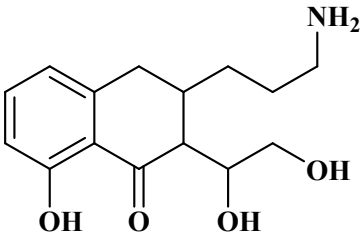

P9

j

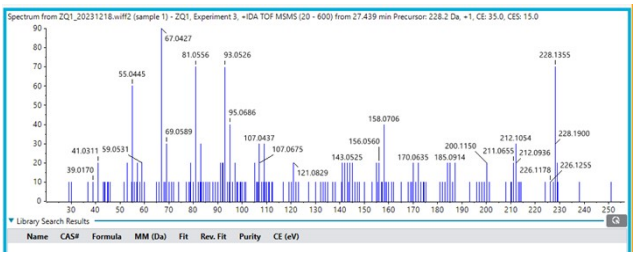

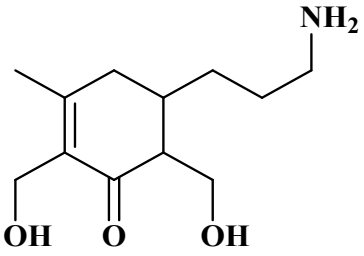

P10

k

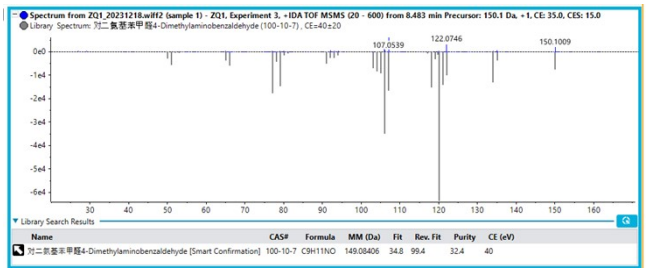

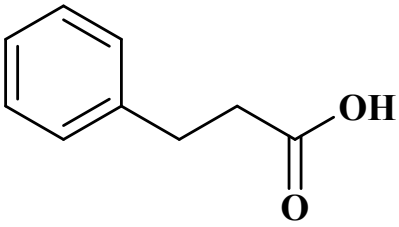

P11

Fig.S3. MS/MS spectra of products detected by UHPLC-QTOF/MS.

Reference

[1] Efficiency of ab-initio total energy calculations for metals and semiconductors using a plane-wave basis set.

[2] Projector augmented-wave method.

[3] G. Zhao, J. Ding, J. Ren, Q. Zhao, Q. Gao, K. Wang, L. Wei, X. Chen, F. Zhou, D.D. Dionysiou, Insight into the visible light activation of sulfite by Fe/g-C_3N_4 with rich N vacancies for pollutant removal and sterilization: A novel approach for enhanced generation of oxysulfur radical, Chem. Eng. J. 438 (2022). https://doi.org/10.1016/j.cej.2022.135663.

[4] W. Tang, E. Sanville, G. Henkelman, A grid-based Bader analysis algorithm without lattice bias, J. Phys. Condens. Mat. 21(8) (2009). https://doi.org/10.1088/0953-8984/21/8/084204.

[5] S. Grimme, J. Antony, S. Ehrlich, H. Krieg, A consistent and accurateab initioparametrization of density functional dispersion correction (DFT-D) for the 94 elements H-Pu, The Journal of Chemical Physics 132(15) (2010). https://doi.org/10.1063/1.3382344.

[6] P. Zhang, Y. Yang, X. Duan, Y. Liu, S. Wang, Density Functional Theory Calculations for Insight into the Heterocatalyst Reactivity and Mechanism in Persulfate-Based Advanced Oxidation Reactions, ACS Catal. 11(17) (2021) 11129-11159. https://doi.org/10.1021/acscatal.1c03099.